Vibronic Ground State Rotational Spectrum of 3-Bromothiophene

Quadrupole Hyperfine Structure and Centrifugal Distortion Analysis

Dirk Hübner, Eckhard Fliege, and Dieter H. Sutter
Institut für Physikalische Chemie der Christian-Albrechts-Universität

Z. Naturforsch. **38 a,** 1238–1247 (1983); received August 29, 1983

The rotational spectrum of 3-bromothiophene was investigated in the frequency range between 8 and 18 GHz by use of a microwave Fourier transform spectrometer. Both *a*- and *b*-type spectra were assigned for the vibronic ground state. Rotational constants, quartic centrifugal distortion constants and quadrupole coupling constants were obtained for the ^{79}Br- and ^{81}Br-isotopic species. For the analysis, the effective rotational Hamiltonian including centrifugal distortion in the form of Van Eijck's symmetric top reduction and bromine quadrupole coupling was set up in the coupled basis of the limiting symmetric top, $|J, K, I, F, M_F\rangle$, and was diagonalized numerically. Spin rotation interaction was neglected.

Introduction

The investigation of the rotational spectrum of 3-bromothiophene was initiated because of our current interest in the effects of halogen substitution on the magnetic properties of aromatic rings [1, 2, 3]. In the following we present a high resolution study of the vibronic ground state rotational spectra of $^{12}C_4{}^1H_3{}^{32}S{}^{79}Br$ and of $^{12}C_4{}^1H_3{}^{32}S{}^{81}Br$. In the final stages of this work we became aware of a similar study carried out recently by Sasada, Saitoh, and Tobita [4]. However, due to the superior performance of the microwave Fourier transform spectrometer used in our work, our data, which include the analysis of the weak μ_b-type spectra and a complee centrifugal distortion analysis up to fourth order, are considerably more accurate and more complete.

Experimental

Commercial 3-bromothiophene (EGA-Chemie) was used after several bulp to bulp distillations without further purification. Since the standard Stark spectra appeared comparatively weak, we switched to the Fourier transform spectrometer developed by Dreizler and coworkers [5] in order to exploit its higher sensitivity and resolution. Typical recording conditions were temperatures about −55 °C and pressures about 1 mtorr.

Reprint requests to Prof. Dr. D. H. Sutter, Institut für Physikalische Chemie, Christian-Albrechts-Universität, Olshausenstr. 40, D-2300 Kiel, Germany.

In Fig. 1 we present a Fourier transform spectrum of the quadrupole hyperfine pattern of the $4_{13} \rightarrow 5_{14}$ rotational transition of $^{12}C_4{}^1H_3{}^{32}S{}^{79}Br$. This spectrum is typical for the signal to noise ratio and the spectral resolution achieved in the present investigation. For comparison we also show a computer simulation of the quadrupole hyperfine structure in the standard absorption spectrum. The latter was calculated from our final data for the quadrupole coupling constants, rotational constants and centrifugal distortion constants (see below). The discrepancy between the relative intensity patterns in the Fourier transform spectrum and in the standard absorption spectrum is obvious. This is however a common feature of microwave Fourier transform spectroscopy and reflects the fact that the polarization efficiency of the exciting microwave pulse is not the same for the different satellites.

Apart from the dipole transition matrix element, the polarization efficiency also depends on the power and duration of the microwave pulse and on the frequency offset between the resonance frequency of the individual transition and the carrier frequency in the exciting pulse [6]. As a result of such differences in the initial polarizations, the intensities of the subsequent transient molecular emission signals do not any more directly reflect the dipole matrix elements and statistical weight factors as would be the case in a standard absorption spectrum.

Throughout the present investigation the transient i. f. signals corresponding to the molecular emission signals were digitized at a rate of 50 MHz (20 ns per

0340-4811 / 83 / 1100-1238 $ 01.3 0/0. – Please order a reprint rather than making your own copy.

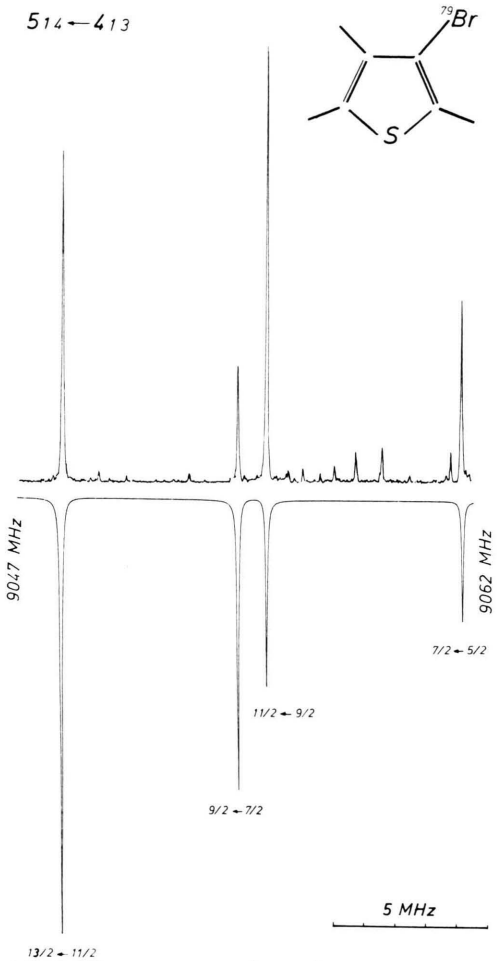

Fig. 1. The upper trace shows the power spectrum for the central section of the ^{79}Br quadrupole hyperfine multiplet of the $^{12}C_4{}^1H_3{}^{32}S^{79}Br$ $5_{14} \rightarrow 4_{13}$ rotational transition. The time domain signal consisted of 1024 data points taken at 20 ns per point after a delay of 0.5 μs to allow pulse echoes to die out. The pulse duration was 90 ns. The carrier frequency in the exciting pulse was 9057 MHz. Eight times 256 k successive free induction decay signals were sampled in order to improve the signal to noise ratio. 3072 zeros were added before Fourier transforming. Pressure: 1.12 mTorr. Temperature: − 56 °C. The lower trace shows a computer simulation calculated according to Eq. (1) from the quadrupole coupling constants, rotational constants and centrifugal distortion constants listed in Tables 3 and 4. The experimental linewidth is 80 kHz full width at half height. „Wrong" relative intensities in the experimental spectrum are partly due to the frequency-offset dependence of the polarization efficiency of the pulse.

data point) and 1024 subsequent data points were taken per experiment. Typically the signals of $2.56 \cdot 10^5$ to $2.05 \cdot 10^6$ repetitive transient emissions were sampled and the final data sequence was incremented by 3072 zeros before the Fourier transformation was carried out. The rate of digitization (20 ns per data point) and the number of points (1024 + 3072) results in a meshwidth of $\Delta\nu = 1/(4096 \cdot 20 \cdot 10^{-9})$ Hz $\cong$ 12.2 kHz in the grid of the discrete Fourier transform spectrum [7], which is still reasonably below the observed linewidth of 80 to 100 kHz. The final satellite frequencies listed in Tables 1 and 2 were calculated from a three point interpolation around the line centers. Due to the limited signal to noise ratio we estimate their precision to 6 kHz for the more intense satellites and to about 12 kHz for the weaker satellites.

Analysis of the spectrum

Initial rotational constants were calculated under the assumption of an undisturbed thiophene ring [8] with a bromine atom substituted in the β-position. The C−Br bond distance, 1.85 Å, was taken from bromobenzene [9]. In Fig. 2 we show this structure and the principal inertia axes system for the ^{79}Br isotopic species. The position and orientation of the principal inertia axes system is largely determined by the position of the bromine atom which accounts for about half the mass of the whole molecule.

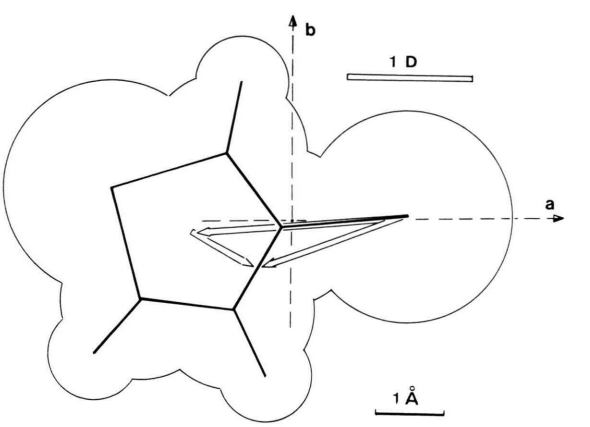

Fig. 2. Approximate structure and dipole moments of ^{79}Br-3-bromothiophene based on an undistorted thiophene ring [8], a C−Br bondlength of 1.85 Å taken from bromobenzene [9] and a vector addition of the experimental dipole moments of thiophene [10] and bromobenzene [11]. Also shown is the position and orientation of the principal inertia axes system. The atomic (a, b)-coordinates of this approximate structure are (− 2.605, 0.517) for the sulfur atom; (− 0.962, 1.005), (− 0.119, − 0.074), (− 0.821, − 1.313) and (− 2.180, − 1.143) for the carbon atoms; (− 0.714, 2.053), (− 0.344, − 2.283) and (− 2.952, − 1.895) for the hydrogen atoms and (1.727, 0.050) for the ^{79}Br-atom. (All values in Å units.) The resulting rigid rotor rotational constants, A = 7178.79 MHz, B = 939.06 MHz and C = 830.43 MHz differ at most by 1% from the experimental values listed in Table 4.

Table 1. Observed and calculated rotational transition frequencies for $^{12}C_4{}^1H_3{}^{79}Br^{32}S$. The calculated frequencies are based on the rotational constants, centrifugal distortion constants and ^{79}Br quadrupole coupling constants listed in Tables 3 and 4 respectively. They were obtained from a complete diagonalization of the Hamiltonian matrix corresponding to Eq. (1) of the text. Also given for comparison are the rigid rotor frequencies ν_{RR} calculated from $\hat{\mathscr{H}}_{RR}/h$ only and the hypothetical „center frequencies" [17] of the hyperfine multiplets, ν_{CD}, calculated from $(\hat{\mathscr{H}}_{RR} + \hat{\mathscr{H}}_{CD})/h$.

Rotational transitions ν_{RR} ν_{CD}	$F' \leftarrow F''$		ν_{obs}/MHz	ν_{calc}/MHz	$\nu_{obs} - \nu_{calc}$ kHz
5 1 5 4 1 4	13/2	11/2	8 506.250	8 506.258	−8
8 511.305 MHz	11/2	9/2	8 513.038	8 513.042	−4
8 511.290 MHz	9/2	7/2	8 519.147	8 519.157	−10
	7/2	5/2	8 511.803	8 511.829	−26
5 1 4 4 1 3	13/2	11/2	9 048.417	9 048.414	3
9 053.505 MHz	11/2	9/2	9 055.205	9 055.208	−3
9 053.488 MHz	9/2	7/2	9 061.646	9 061.644	2
	7/2	5/2	9 054.275	9 054.277	−2
5 2 4 4 2 3	13/2	11/2	8 773.602	8 773.613	−11
8 785.459 MHz	11/2	9/2	8 801.401	8 801.395	6
8 785.435 MHz	9/2	7/2	8 798.032	8 798.033	−1
	7/2	5/2	8 768.267	8 768.288	−21
5 2 3 4 2 2	13/2	11/2	8 801.769	8 801.766	3
8 813.750 MHz	11/2	9/2	8 829.704	8 829.706	−2
8 813.726 MHz	9/2	7/2	8 826.369	8 826.374	−5
	7/2	5/2	8 796.499	8 796.509	−10
6 0 6 5 0 5	15/2	13/2	10 494.924	10 494.915	9
10 496.961 MHz	13/2	11/2	10 494.688	10 494.702	−14
10 496.938 MHz	11/2	9/2	10 500.976	10 500.972	4
	9/2	7/2	10 501.224	10 501.214	10
6 1 6 5 1 5	15/2	13/2	10 206.393	10 206.395	−2
10 209.842 MHz	13/2	11/2	10 210.274	10 210.263	11
10 209.819 MHz	11/2	9/2	10 214.922	10 214.925	−3
	9/2	7/2	10 210.811	10 210.827	−16
6 1 5 5 1 4	15/2	13/2	10 856.631	10 856.634	−3
10 860.126 MHz	13/2	11/2	10 860.502	10 860.504	−2
10 860.097 MHz	11/2	9/2	10 865.463	10 865.471	−8
	9/2	7/2	10 861.308	10 861.312	−4
6 2 5 5 2 4	15/2	13/2	10 532.304	10 532.306	−2
10 539.952 MHz	13/2	11/2	10 548.157	10 548.157	0
10 539.916 MHz	11/2	9/2	10 548.596	10 548.594	2
	9/2	7/2	10 531.676	10 531.686	−10
6 2 4 5 2 3	15/2	13/2	10 581.583	10 581.587	−4
10 589.321 MHz	13/2	11/2	10 597.573	10 597.579	−6
10 589.284 MHz	11/2	9/2	10 598.017	10 598.027	−10
	9/2	7/2	10 580.969	10 580.974	−5
6 3 3 5 3 2	15/2	13/2	10 539.733	10 539.776	−3
10 554.460 MHz	13/2	11/2	10 575.891	10 575.890	1
10 554.408 MHz	11/2	9/2	10 568.653	10 568.655	−2
	9/2	7/2	10 530.875	10 530.885	−10
6 4 3 5 4 2	15/2	13/2	10 526.495	10 526.496	−1
6 4 2 5 4 1	13/2	11/2	10 591.500	10 591.498	2
10 551.154 MHz	11/2	9/2	10 572.772	10 572.774	−2
10 551.079 MHz	9/2	7/2	10 506.780	10 506.788	−8
6 5 2 5 5 1	15/2	13/2	10 512.134	10 512.138	−4
6 5 1 5 5 0	13/2	11/2	10 615.355	10 615.349	6
10 549.879 MHz	11/2	9/2	10 580.513	10 580.519	−6
10 549.775 MHz	9/2	7/2	10 479.731	10 479.751	−20
7 0 7 6 0 6	17/2	15/2	12 223.858	12 223.861	−3
12 225.418 MHz	15/2	13/2	12 223.647	12 223.655	−8
12 225.383 MHz	13/2	11/2	12 228.143	12 228.150	−7
	11/2	9/2	12 228.375	12 228.378	−3
7 1 7 6 1 6	17/2	15/2	11 903.946	11 903.947	−1
11 906.450 MHz	15/2	13/2	11 906.352	11 906.353	−1
11 906.415 MHz	13/2	11/2	11 910.101	11 901.103	−2
	11/2	9/2	11 907.509	11 907.511	−2
7 2 6 6 2 5	17/2	15/2	12 287.745	12 287.746	−1
12 293.028 MHz	15/2	13/2	12 297.647	12 297.647	0
12 292.977 MHz	13/2	11/2	12 299.090	12 299.094	−4
	11/2	9/2	12 288.583	12 288.589	−6
7 2 5 6 2 4	17/2	15/2	12 366.323	12 366.327	−4
12 371.655 MHz	15/2	13/2	12 376.378	12 376.380	−2
12 371.602 MHz	13/2	11/2	12 377.797	12 377.801	−4
	11/2	9/2	12 367.120	12 367.125	−5
7 3 5 6 3 4	17/2	15/2	12 305.230	12 305.231	−1
12 315.124 MHz	15/2	13/2	12 327.743	12 327.746	−3
12 315.053 MHz	13/2	11/2	12 325.220	12 325.216	4
	11/2	9/2	12 301.591	12 301.598	−7
7 3 4 6 3 3	17/2	15/2	12 306.671	12 306.672	−1
12 316.582 MHz	15/2	13/2	12 329.193	12 329.203	−10
12 316.511 MHz	13/2	11/2	12 326.678	12 326.677	1
	11/2	9/2	12 303.046	12 303.052	−6
7 4 4 6 4 3	17/2	15/2	12 294.663	12 294.660	3
7 4 3 6 4 2	15/2	13/2	12 335.022	12 335.021	1
12 311.111 MHz	13/2	11/2	12 326.679	12 326.684	−5
12 311.014 MHz	11/2	9/2	12 285.116	12 285.117	−1
7 5 3 6 5 2	17/2	15/2	12 284.132	12 284.135	−3
7 5 2 6 5 1	15/2	13/2	12 347.826	12 347.828	−2
12 309.088 MHz	13/2	11/2	12 331.483	12 331.488	−5
12 308.957 MHz	11/2	9/2	12 267.406	12 267.416	−10
7 6 2 6 61	17/2	15/2	12 272.504	12 272.508	−4
7 6 1 6 6 0	15/2	13/2	12 365.355	12 365.356	−1
12 308.027 MHz	13/2	11/2	12 338.440	12 338.443	−3
12 307.854 MHz	11/2	9/2	12 247.694	12 247.710	−16
7 1 7 6 0 6	17/2	15/2	17 071.313	17 071.315	−2
17 069.239 MHz	15/2	13/2	17 062.281	17 062.284	−3
17 069.196 MHz	13/2	11/2	17 068.479	17 068.483	−4
	11/2	9/2	17 077.818	17 077.829	−11
8 1 7 8 0 8	19/2	19/2	8 401.752	8 401.749	3
8 400.333 MHz	17/2	17/2	8 398.271	8 398.271	0
8 400.291 MHz	15/2	15/2	8 398.699	8 398.700	−1
	13/2	13/2	8 402.363	8 402.369	−6
8 0 8 7 1 7	19/2	17/2	9 095.946	9 095.949	−3
9 100.810 MHz	17/2	15/2	9 104.562	9 104.564	−2
9 100.766 MHz	15/2	13/2	9 106.291	9 106.292	−1
	13/2	11/2	9 097.375	9 097.388	−13
8 0 8 7 0 7	19/2	17/2	13 943.398	13 943.401	−3
13 944.631 MHz	17/2	15/2	13 943.184	13 943.191	−7
13 944.578 MHz	15/2	13/2	13 946.612	13 946.624	−12
	13/2	11/2	13 946.833	13 946.837	−4
8 1 8 7 1 7	19/2	17/2	13 598.982	13 598.984	−2
13 600.892 MHz	17/2	15/2	13 600.572	13 600.573	−1
13 600.840 MHz	15/2	13/2	13 603.463	13 603.465	−2
	13/2	11/2	13 601.789	13 601.790	−1

Table 1 (continued)

Rotational transitions ν_{RR} ν_{CD}	$F' \leftarrow F''$	ν_{obs}	ν_{calc}	$\nu_{obs}-\nu_{calc}$
8 1 7 7 1 6	19/2 17/2	14 463.940	14 463.945	−5
14 465.888 MHz	17/2 15/2	14 465.509	14 465.512	−3
14 465.823 MHz	15/2 13/2	14 468.524	14 468.530	−6
	13/2 11/2	14 466.841	14 466.848	−7
8 2 6 8 1 7	19/2 19/2	17 053.078	17 053.080	−2
17 045.217 MHz	17/2 17/2	17 034.486	17 034.482	4
17 045.134 MHz	15/2 15/2	17 037.581	17 037.586	−5
	13/2 13/2	17 056.596	17 056.588	8
8 2 7 7 2 6	19/2 17/2	14 040.604	14 040.608	−4
14 044.453 MHz	17/2 15/2	14 047.195	14 047.202	−7
14 044.383 MHz	15/2 13/2	14 048.836	14 048.839	−3
	13/2 11/2	14 041.872	14 041.876	−4
8 2 6 7 2 5	19/2 17/2	14 157.736	14 157.738	−2
14 161.574 MHz	17/2 15/2	14 164.417	14 164.422	−5
14 161.499 MHz	15/2 13/2	14 166.106	14 166.110	−4
	13/2 11/2	14 158.887	14 158.894	−7
8 3 6 7 3 5	19/2 17/2	14 070.223	14 070.228	−5
14 077.361 MHz	17/2 15/2	14 085.264	14 085.266	−2
14 077.267 MHz	15/2 13/2	14 084.680	14 084.684	−4
	13/2 11/2	14 068.937	14 068.954	−17
8 3 5 7 3 4	19/2 17/2	14 073.145	14 073.147	−2
14 080.274 MHz	17/2 15/2	14 088.180	14 088.189	−9
14 080.180 MHz	15/2 13/2	14 087.595	14 087.601	−6
	13/2 11/2	14 071.846	14 071.862	−16
8 4 5 7 4 4	19/2 17/2	14 060.135	14 060.138	−3
8 4 4 7 4 3	17/2 15/2	14 086.973	14 086.975	−2
14 071.739 MHz	15/2 13/2	14 083.080	14 083.081	−1
14 071.615 MHz	13/2 11/2	14 055.298	14 055.300	−2
8 5 4 7 5 3	19/2 17/2	14 051.245	14 051.250	−5
8 5 3 7 5 2	17/2 15/2	14 093.453	14 093.458	−5
14 068.712 MHz	15/2 13/2	14 085.114	14 085.126	−12
14 068.549 MHz	13/2 11/2	14 042.085	14 042.096	−11
8 6 3 7 6 2	19/2 17/2	14 042.410	14 042.417	−7
8 6 2 7 6 1	17/2 15/2	14 103.687	14 103.693	−6
14 067.127 MHz	15/2 13/2	14 089.586	14 089.588	−2
14 066.916 MHz	13/2 11/2	14 028.277	14 028.287	−10
8 7 2 7 7 1	19/2 17/2	14 032.810	14 032.800	10
8 7 1 7 7 0	17/2 15/2	14 117.007	14 117.012	−5
14 066.190 MHz	15/2 13/2	14 095.592	14 095.590	2
14 065.924 MHz	13/2 11/2	14 013.193	14 013.208	−15

Table 2. Observed and calculated rotational transition frequencies for $^{12}C_4{}^{1}H_3{}^{81}Br^{32}S$.

Rotational transition ν_{RR} ν_{CD}	$F' \leftarrow F''$	ν_{obs}/MHz	ν_{calc}/MHz	$\nu_{obs}-\nu_{calc}$/kHz
5 1 5 4 1 4	13/2 11/2	8 422.620	8 422.625	−5
8 426.869 MHz	11/2 9/2	8 428.328	8 428.337	−9
8 426.856 MHz	9/2 7/2	8 433.443	8 433.456	−13
	7/2 5/2	8 427.336	8 427.363	−7
5 1 4 4 1 3	13/2 11/2	8 953.802	8 953.807	−5
8 958.092 MHz	11/2 9/2	8 959.517	8 959.523	−6
8 958.075 MHz	9/2 7/2	8 964.895	8 964.906	−11
	7/2 5/2	8 958.773	8 958.781	−8
5 2 4 4 2 3	13/2 11/2	8 685.433	8 685.466	−33
8 695.408 MHz	11/2 9/2	8 708.734	8 708.778	−44
8 695.386 MHz	9/2 7/2	8 705.828	8 705.865	−37
	7/2 5/2	8 681.138	8 681.169	−31
5 2 3 4 2 2	13/2 11/2	8 712.495	8 712.491	4
8 722.530 MHz	11/2 9/2	8 735.923	8 735.921	2
8 722.507 MHz	9/2 7/2	8 733.030	8 733.027	3
	7/2 5/2	8 708.255	8 708.233	22
6 0 6 5 0 5	15/2 13/2	10 389.059	10 389.052	7
10 390.778 MHz	13/2 11/2	10 388.878	10 388.883	−5
10 390.757 MHz	11/2 9/2	10 394.160	10 394.161	−1
	9/2 7/2	10 394.347	10 394.342	5
6 1 6 5 1 5	15/2 13/2	10 105.772	10 105.769	3
10 108.670 MHz	13/2 11/2	10 109.027	10 109.026	1
10 108.648 MHz	11/2 9/2	10 112.964	10 112.955	9
	9/2 7/2	10 109.527	10 109.528	−1
6 1 5 5 1 4	15/2 13/2	10 742.859	10 742.863	−4
10 745.803 MHz	13/2 11/2	10 746.119	10 746.119	0
10 745.775 MHz	11/2 9/2	10 750.273	10 750.277	−4
	9/2 7/2	10 746.808	10 746.815	−7
6 2 5 5 2 4	15/2 13/2	10 425.572	10 425.578	−6
10 431.998 MHz	13/2 11/2	10 438.881	10 438.882	−1
10 431.965 MHz	11/2 9/2	10 439.196	10 439.197	−1
	9/2 7/2	10 425.143	10 425.150	−7
6 2 4 5 2 3	15/2 13/2	10 472.838	10 472.839	−1
10 479.333 MHz	13/2 11/2	10 486.256	10 486.257	−1
10 479.298 MHz	11/2 9/2	10 486.580	10 486.582	−2
	9/2 7/2	10 472.404	10 472.417	−13
6 3 3 5 3 2	15/2 13/2	10 433.582	10 433.586	−4
10 445.899 MHz	13/2 11/2	10 463.845	10 463.846	−1
10 445.849 MHz	11/2 9/2	10 457.691	10 457.696	−5
	9/2 7/2	10 426.264	10 426.269	−5
6 4 3 5 4 2	15/2 13/2	10 422.091	10 422.094	−3
6 4 2 5 4 1	13/2 11/2	10 476.450	10 476.451	−1
10 442.738 MHz	11/2 9/2	10 460.721	10 460.723	−2
10 442.665 MHz	9/2 7/2	10 405.670	10 405.672	−2
6 5 2 5 5 1	15/2 13/2	10 409.987	10 409.980	7
6 5 1 5 5 0	13/2 11/2	10 496.064	10 496.067	−3
10 441.514 MHz	11/2 9/2	10 467.070	10 467.088	−18
10 441.413 MHz	9/2 7/2	10 382.726	10 382.724	2

Table 2 (continued)

Rotational transition ν_{RR} ν_{CD}	$F' \leftarrow F''$	ν_{obs}/MHz	ν_{calc}/MHz	$\nu_{obs}-\nu_{calc}$/kHz
7 0 7 6 0 6	17/2 15/2	12 101.079	12 101.074	−5
12 102.391 MHz	15/2 13/2	12 100.908	12 100.911	−3
12 102.357 MHz	13/2 11/2	12 104.687	12 104.693	−6
	11/2 9/2	12 104.869	12 104.869	0
7 1 7 6 1 6	17/2 15/2	11 786.514	11 786.510	4
11 788.618 MHz	15/2 13/2	11 788.540	11 788.535	5
11 788.585 MHz	13/2 11/2	11 791.655	11 791.660	−5
	11/2 9/2	11 789.516	11 789.513	3
7 2 6 6 2 5	17/2 15/2	12 162.780	12 162.791	−11
12 167.231 MHz	15/2 13/2	12 171.098	12 171.101	−3
12 167.182 MHz	13/2 11/2	12 172.281	12 172.286	−5
	11/2 9/2	12 163.542	12 163.550	−8
7 2 5 6 2 4	17/2 15/2	12 238.156	12 238.157	−1
12 242.632 MHz	15/2 13/2	12 246.588	12 246.592	−4
12 242.581 MHz	13/2 11/2	12 247.754	12 247.751	3
	11/2 9/2	12 238.873	12 238.878	−5
7 3 5 6 3 4	17/2 15/2	12 180.112	12 180.114	−2
12 188.426 MHz	15/2 13/2	12 198.989	12 198.991	−2
12 188.358 MHz	13/2 11/2	12 196.810	12 196.818	−8
	11/2 9/2	12 177.162	12 177.168	−6
7 3 4 6 3 3	17/2 15/2	12 181.472	12 181.474	−2
12 189.793 MHz	15/2 13/2	12 200.353	12 200.358	−5
12 189.725 MHz	13/2 11/2	12 198.188	12 198.188	0
	11/2 9/2	12 178.523	12 178.532	−9
7 4 4 6 4 3	17/2 15/2	12 170.779	12 170.779	0
7 4 3 6 4 2	15/2 13/2	12 204.566	12 204.561	5
12 184.570 MHz	13/2 11/2	12 197.515	12 197.510	5
12 184.476 MHz	11/2 9/2	12 162.880	12 162.878	2
7 5 3 6 5 2	17/2 15/2	12 161.740	12 161.743	−3
7 5 2 6 5 1	15/2 13/2	12 214.974	12 214.976	−2
12 182.626 MHz	13/2 11/2	12 201.277	12 201.280	−3
12 182.499 MHz	11/2 9/2	12 147.773	12 147.781	−8
7 6 2 6 6 1	17/2 15/2	12 151.924	12 151.929	−5
7 6 1 6 6 0	15/2 13/2	12 229.381	12 229.378	3
12 181.608 MHz	13/2 11/2	12 207.003	12 207.005	−2
12 181.440 MHz	11/2 9/2	12 131.042	12 131.048	−6
8 1 7 8 0 8	19/2 19/2	8 361.382	8 361.386	−4
8 360.209 MHz	17/2 17/2	–	8 358.463	–
8 360.163 MHz	15/2 15/2	–	8 358.845	–
	13/2 13/2	8 361.900	8 361.900	0
8 0 8 7 1 7	19/2 17/2	8 923.619	8 923.620	−1
8 927.710 MHz	17/2 15/2	8 930.861	8 930.862	−1
8 927.667 MHz	15/2 13/2	8 932.302	8 932.301	1
	13/2 11/2	8 924.855	8 924.863	−8
8 0 8 7 0 7	19/2 17/2	13 804.080	13 804.074	6
13 805.115 MHz	17/2 15/2	13 803.899	13 803.908	−9
13 805.066 MHz	15/2 13/2	13 806.780	13 806.792	−12
	13/2 11/2	13 806.967	13 806.964	3
8 1 8 7 1 7	19/2 17/2	13 464.869	13 464.876	−7
13 466.482 MHz	17/2 15/2	13 466.208	13 466.213	−5
13 466.435 MHz	15/2 13/2	13 468.636	13 468.642	−6
	13/2 11/2	13 467.234	13 467.244	−10
8 1 7 7 1 6	19/2 17/2	14 312.421	14 312.427	−6
14 314.072 MHz	17/2 15/2	14 313.746	14 313.751	−5
14 314.008 MHz	15/2 13/2	14 316.269	14 316.278	−9
	13/2 11/2	14 314.868	14 314.876	−8
8 2 6 8 1 7	19/2 19/2	17 103.483	17 103.486	−3
17 096.937 MHz	17/2 17/2	17 087.920	17 087.919	1
17 096.860 MHz	15/2 15/2	17 090.546	17 090.543	3
	13/2 13/2	17 106.421	17 106.419	2
8 2 7 7 2 6	19/2 17/2	13 897.640	13 897.645	−5
13 900.880 MHz	17/2 15/2	13 903.176	13 903.179	−3
13 900.813 MHz	15/2 13/2	13 904.532	13 904.536	−4
	13/2 11/2	13 898.739	13 898.743	−4
8 2 6 7 2 5	19/2 17/2	14 009.961	14 009.971	−10
14 013.229 MHz	17/2 15/2	14 015.599	14 015.606	−7
14 013.157 MHz	15/2 13/2	14 016.981	14 016.988	−7
	13/2 11/2	14 010.998	14 011.006	−8
8 3 6 7 3 5	19/2 17/2	13 926.471	13 926.476	−5
13 932.454 MHz	17/2 15/2	13 939.076	13 939.074	2
13 932.364 MHz	15/2 13/2	13 938.532	13 938.544	−12
	13/2 11/2	13 925.435	13 925.455	−20
8 3 5 7 3 4	19/2 17/2	13 929.206	13 929.206	0
13 935.187 MHz	17/2 15/2	13 941.793	13 941.810	−17
13 935.096 MHz	15/2 13/2	13 941.302	13 941.278	24
	13/2 11/2	13 928.170	13 928.181	−11
8 4 5 7 4 4	19/2 17/2	13 917.306	13 917.306	0
8 4 4 7 4 3	17/2 15/2	13 939.772	13 939.781	−9
13 927.036 MHz	15/2 13/2	13 936.454	13 936.465	−11
13 926.916 MHz	13/2 11/2	13 913.314	13 913.326	−12
8 5 4 7 5 3	19/2 17/2	13 909.498	13 909.503	−5
8 5 3 7 5 2	17/2 15/2	13 944.811	13 944.813	−2
13 924.134 MHz	15/2 13/2	13 937.785	13 937.789	−4
13 923.976 MHz	13/2 11/2	13 901.912	13 901.899	13
8 6 3 7 6 2	19/2 17/2	13 901.912	13 901.934	−22
8 6 2 7 6 1	17/2 15/2	13 953.124	13 953.129	−5
13 922.615 MHz	15/2 13/2	13 941.302	13 941.327	−25
13 922.410 MHz	13/2 11/2	13 890.106	13 890.115	−9
8 7 2 7 7 1	19/2 17/2	13 893.806	13 893.807	−1
8 7 1 7 7 0	17/2 15/2	13 964.047	13 964.061	−14
13 921.717 MHz	15/2 13/2	13 946.282	13 946.260	22
13 921.458 MHz	13/2 11/2	13 877.284	13 877.302	−18

The molecular *a*-axis (= axis of least moment of inertia) almost coincides with the C−Br bond and inspite of their disque shaped geometry both 3-bromothiophenes, as far as their rotational energy level patterns are concerned, closely correspond to prolate symmetric tops with the *a*-axes as symmetry axes of the moment of inertia tensor.

Also shown in Fig. 2 is a prediction for the electric dipole moment vector. It was calculated as sum vector from the experimental dipole moments of

thiophene ($\mu = 0.55$ Debye [10]) and bromobenzene ($\mu = 1.7$ Debye [11]). With the predicted μ_a-value roughly three times μ_b, the rotational spectra were expected to be dominated by μ_a-type transitions with groups of lines corresponding to the $\Delta J = +1$, $\Delta K = 0$ transitions of the limiting prolate symmetric top.

Such groups of lines were indeed found at frequency intervals of approximately 1.7 GHz which roughly corresponds to the sum of the B and C rotational constants. The final assignment of the individual transitions within these groups was quickly established due to their typical bromine quadrupole hyperfine structure which could be predicted from the known quadrupole coupling constants of 3-bromofurane [12]. The assignment was confirmed by the excellent selfconsistency of the fit.

In Tables 1 and 2 we list the assigned transitions for the two most abundant isotopic species, $^{12}C_4{}^1H_3{}^{32}S^{79}Br$ (ca. 45.9%) and $^{12}C_4{}^1H_3{}^{32}S^{81}Br$ (ca. 44.9%) respectively. Both lists include several of the weak μ_b-transitions. This greatly reduces the experimental uncertainties in the A rotational constant.

For the final analysis we used the effective rotational Hamiltonian given in (1). It includes centrifugal distortion corrections up to quartic terms in the angular momentum operators and results from a second order perturbation treatment within the vibronic system which aims at the vibronic ground state [13].

Since as far as its rotational constants are concerned 3-bromothiophene comes close to a prolate symmetric top, the centrifugal distortion part of the Hamiltonian was arranged according to the "symmetric-top-reduction" proposed by Van Eijck [14] (Eq. (10) of [14]).

$$\begin{aligned}\hat{\mathscr{H}}_{\text{eff}}/h = {} & A' \cdot \hat{J}_a^2 + B' \cdot \hat{J}_b^2 + C' \cdot \hat{J}_c^2 && \} \hat{\mathscr{H}}_{\text{RR}}/h \\ & \left.\begin{aligned} & - D'_J \cdot \hat{J}^4 - D'_{JK} \cdot \hat{J}^2 \hat{J}_a^2 - D'_K \cdot \hat{J}_a^4 \\ & - 2 \cdot \delta'_J \cdot \hat{J}^2 (\hat{J}_b^2 - \hat{J}_c^2) \\ & - 2 \cdot R'_6 \cdot [3 (\hat{J}_b^2 \cdot \hat{J}_c^2 + \hat{J}_c^2 \hat{J}_b^2) - \hat{J}_b^4 - \hat{J}_c^4] \end{aligned}\right\} \hat{\mathscr{H}}_{\text{CD}}/h \\ & + \frac{1}{4} \sum_{m=-2}^{2} (-1)^m Q_m^{(2)} \cdot V_{-m}^{(2)} && \} \hat{\mathscr{H}}_{\text{Q}}/h\,. \end{aligned} \tag{1}$$

In Eq. (1) the indices a, b and c designate the principal inertia axes system of the rotating molecule.

A', B', C' are effective rotational constants measured in frequency units.

$\hat{J}_a, \hat{J}_b, \hat{J}_c$ are the angular momentum operators corresponding to the components of the angular momentum with respect to the molecular axes system measured in units of $\hbar$.

D'_J, D'_{JK}, D'_K are centrifugal distortion constants.

δ'_J, R'_6 They too are measured in frequency units. For their defintion the reader is referred to [14].

In Eq. (1) the quadrupole coupling operator is expressed in spherical tensor notation. The Qm's and Vm's are defined as follows [15]:

$$\begin{aligned} Q_0^{(2)} &= Q_{ZZ}\,, \\ Q_{\pm 1}^{(2)} &= \mp \sqrt{\frac{2}{3}}\,(Q_{XZ} \pm i\,Q_{YZ})\,, \\ Q_{\pm 2}^{(2)} &= \frac{1}{\sqrt{6}}\,(Q_{XX} - Q_{YY} \pm 2i\,Q_{XY})\,, \\ V_0^{(2)} &= V_{ZZ}\,, \\ V_{\pm 1}^{(2)} &= \mp \sqrt{\frac{2}{3}}\,(V_{XZ} \pm i\,V_{YZ})\,, \\ V_{\pm 2}^{(2)} &= \frac{1}{\sqrt{6}}\,(V_{XX} - V_{YY} \pm 2i\,V_{XY})\,. \end{aligned} \tag{2}$$

Here the indices X, Y, Z designate the space fixed axes of the laboratory system with the Z-axis in direction of the electric field vector of the incident microwave radiation. $Q_{FF'}$, ($F, F' = X, Y, Z$) are the elements of the bromine nuclear quadrupole moment tensor. Within a classical point charge model for the nucleus they correspond to the following expressions:

$$Q_{FF'} = \sum_n e_n [\tfrac{3}{2} (F_n \cdot F'_n + F'_n \cdot F_n) - \delta_{FF'} \cdot R_n^2] \tag{3}$$

with $R_n^2 = X_n^2 + Y_n^2 + Z_n^2$, $\delta_{FF'}$ the Kronecker symbol and e_n the electric charge of the n-th point charge within the nucleus. We note that some authors use a definition of the quadrupole moment which differs by a factor of 1/2 from the definition used here.

$V_{FF'}$ are the second derivatives of the intramolecular Coulomb potential V with respect to the space fixed aces. They are taken at the position of the bromine nucleus. Only that part of V is con-

sidered which originates from charges outside the nucleus.

$$V_{FF'} = \sum_{\varepsilon} R_{\varepsilon}^{-5} e_{\varepsilon} [\tfrac{3}{2} (F_{\varepsilon} F'_{\varepsilon} + F'_{\varepsilon} F_{\varepsilon}) - \delta_{FF'} R_{\varepsilon}^{2}] . \quad (4)$$

In (3) and (4) all coordinates are referred to an axes system parallel to the space fixed laboratory system but with its origin at the center of the quadrupole nucleus.

For the numerical analysis the matrix of the Hamiltonian given in (1) was set up in the coupled basis corresponding to the limiting symmetric top $|J, K_-, I, F, M_F\rangle$ [16]. This matrix factorizes into F-blocks (F = quantum number corresponding to the overall angular momentum including the spin of the Bromine nucleus (I) and the rotational angular momentum (J), but neglecting all other spins). In the case of the Br-nuclei with nuclear spin $I = 3/2$, each F-block comprises contributions from four J-blocks and was diagonalized numerically. The rotational constants, the quadrupole coupling constants and the quartic centrifugal distortion constants could be fitted to the observed spectra.

Since the quadrupole coupling constants essentially determine the splitting of the rotational transitions into the $F \to F'$ hyperfine satellites while the centrifugal distortion constants determine the position of the center frequency of the hfs multiplet [17], this fit was carried out in an iterative procedure based on the following three step cycle

1. Only $\hat{\mathscr{H}}_{RR}/h$ (with approximate rotational constants) and $\hat{\mathscr{H}}_{Q}/h$ were used to fit the quadrupole coupling constants to the observed multiplet splittings.
2. With these improved quadrupole coupling constants we calculated the hypothetical quadrupole free rotational transition frequencies (multiplet center frequencies).
3. Only $\hat{\mathscr{H}}_{RR}/h$ and $\hat{\mathscr{H}}_{CD}/h$ together with the multiplet center frequencies determined in step 2 were used for a least squares fit of the rotational constants and of the centrifugal distortion constants.

The improved rotational constants which resulted from step 3 were then used as input data for step 1 of the next cycle.

Selfconsistency was achieved already after two cycles. The results are presented in Table 3 (quadrupole coupling constants) and Table 4 (rotational constants and centrifugal distortion constants). As a check for this numerical procedure we used the data of Tables 3 and 4 as input for a computer program which sets up the matrix of the complete effective Hamiltonian in the coupled symmetric top basis $|J, K_-, I, F, M_F\rangle$ and diagonalizes it numerically [18].

As might be expected from the small centrifugal corrections (below 300 kHz for the low J transitions observed here) both numerical procedures lead (within better than 0.1 kHz) to identical results.

Table 3. Bromine quadrupole coupling constants for the two isotopic species. Only $|\chi_{ab}|$ is determined by the experiment, but a negative sign would correspond to a tilt angle greater than 7° between the C– Br-bond axis and the principal z-axis of the quadrupole coupling tensor which appears highly unlikely. (y-axis perpendicular to the molecular plane). δ, defined in Eq. (6) of the text, is a measure of the double bond contribution to the carbon halogen bond (1.5%). The quadrupole coupling constants relate to the nuclear quadrupole moment and the field-gradients via $\chi_{aa} = \langle I, M_I = I | Q_{zz} | I, M_I = I\rangle \cdot V_{aa}/h$ etc.

	$^{12}C_4{}^1H_3{}^{32}S^{79}Br$	$^{12}C_4{}^1H_3{}^{32}S^{81}Br$
$(\chi_{bb} + \chi_{cc})$/MHz	− 571.60 (1)	− 477.57 (1)
$(\chi_{bb} - \chi_{cc})$/MHz	− 14.37 (3)	− 12.05 (5)
χ_{ab}/MHz	54.1 (6)	47.6 (11)
χ_{xx}/MHz	− 296.36 (10)	− 247.94 (17)
χ_{yy}/MHz	− 278.62 (2)	− 232.76 (3)
χ_{zz}/MHz	574.97 (9)	480.70 (14)
θ_{az}	3.57 (4)°	3.75 (9)°
$\Delta = (\chi_{xx} - \chi_{yy})$/MHz	− 17.74	− 15.18
$\eta = (\chi_{xx} - \chi_{yy})/\chi_{zz}$	− 0.031	− 0.032
δ	0.0154 (1)	0.0157 (2)

Table 4. Rotational constants, asymmetry parameter $\varkappa$, moments of inertia (conversion factor 505.376 MHz amu Å^2), inertia defect and centrifugal distortion constants. (R'_6 follows from the other constants via the planarity condition; see Table 5).

	$^{12}C_4{}^1H_3{}^{32}S^{79}Br$	$^{12}C_4{}^1H_3{}^{32}S^{81}Br$
A'/MHz	7102.6529 (42)	7102.1713 (85)
B'/MHz	933.1055 (5)	922.9881 (7)
C'/MHz	824.6167 (5)	816.6978 (7)
$\varkappa$	− 0.965	− 0.966
I_{aa}/amu Å^2	71.1531	71.1580
I_{bb}/amu Å^2	541.6065	547.5434
I_{cc}/amu Å^2	612.8617	618.8042
$(I_{cc} - I_{aa} - I_{bb})$/amu Å^2	0.102	0.103
D'_J/MHz	$0.27(2) \cdot 10^{-4}$	$0.25(4) \cdot 10^{-4}$
D'_{JK}/MHz	$0.270(4) \cdot 10^{-4}$	$0.265(6) \cdot 10^{-3}$
D'_K/MHz	$0.23(9) \cdot 10^{-2}$	$0.21(19) \cdot 10^{-2}$
δ'_J/MHz	$0.34(28) \cdot 10^{-5}$	$0.40(43) \cdot 10^{-5}$
R'_6 MHz	$-0.5(8) \cdot 10^{-6}$	$-0.7(13) \cdot 10^{-6}$

Table 5. Correlation matrices for the least squares fit of the rotational constants and centrifugal distortion constants (step 3 of the iterative procedure described in the text). Due to the planarity condition [31]: $4C' D'_J - (B' - C') D'_{JK} - 2(2A' + B' + C') \delta'_J - 4(4A' + B' + C') R'_6 = 0$. R'_6 can not be determined independently and the fit was carried out accounting for the planarity condition as described in [32]. V. Typkes program ZFAP4 was used.

3-Brom(79)thiophen							
A'	1.000						
B'	0.264	1.000					
C'	− 0.311	− 0.400	1.000				
D'_J	− 0.046	0.577	0.459	1.000			
D'_{JK}	0.076	− 0.078	0.048	− 0.261	1.000		
D'_K	0.858	− 0.042	− 0.042	− 0.081	0.022	1.000	
δ'_J	0.360	0.811	− 0.816	0.069	− 0.088	0.047	1.000
3-Brom(81)thiophen							
A'	1.000						
B'	0.064	1.000					
C'	− 0.122	− 0.422	1.000				
D'_J	− 0.132	0.588	0.422	1.000			
D'_{JK}	0.221	0.125	0.089	− 0.287	1.000		
D'_K	0.920	− 0.166	0.082	− 0.160	0.186	1.000	
δ'_J	0.226	0.807	− 0.815	0.078	− 0.102	− 0.013	1.000

In fact in Tables 1 and 2 the frequencies labelled „calc" have been calculated from the molecular parameters listed in Tables 3 and 4 by direct diagonalization of the complete Hamiltonian given in (1).

Discussion

In view of the present lack of sufficient data for a complete structure determination from the rotational constants of different isotopic species, we restrict our discussion to some remarks on the observed bromine quadrupole coupling tensor.

From χ_{aa}, χ_{bb} and χ_{ab} we may calculate the quadrupole coupling tensor elements in its principal axes system, x, y, z (y-axis parallel to the molecular c-axis i.e. perpendicular to the molecular plane).

This requires a rotation by an angle

$$\theta_{az} = 1/2 \cdot \arctan(2\,\chi_{ab}/(\chi_{aa} - \chi_{bb}))$$

about the $c = y$ axis and leads to the quadrupole coupling tensor elements in its principal axes system which are listed in Table 3.

Depending on the actual sign of χ_{ab}, θ_{az} would be $\pm 3.6°$ for ^{79}Br-3-bromothiopene (for $\chi_{ab} = \pm 54.1$ MHz) and $\pm 3.8°$ for ^{81}Br-3-bromothiophene (for $\chi_{ab} = \pm 47.6$ MHz). The upper (positive) sign would correspond to a z-axis closely alligned to the CBr bond axis (compare also Fig. 2), while the lower (negative) sign would correspond to a 7° tilt between the C−Br bond axis and the symmetry axis of the quadrupole coupling tensor. Since the quadrupole coupling tensor reflects the symmetry of the close electronic surrounding of the nucleus, a 7° tilt would correspond to a rather extreme banana shaped σ-bond. We are therefore confident that the possibility of a negative sign for χ_{ab} may be discarded.

The asymmetry in the in plane (χ_{xx}) and out of plane (χ_{yy}) quadrupole coupling tensor elements perpendicular to the bond axis (z-axis) may be used as a measure for the degree of double bond character, δ, in the C−Br-bond [19], [20].

$$\delta = \frac{2}{3} \frac{\chi_{xx} - \chi_{yy}}{e\,Q\,q_{n,1,0}}. \tag{5}$$

In (5) the denominator $e\,Q\,q_{n,1,0}$ represents the quadrupole coupling contribution of an electron in the atomic bromine p_z valence orbital ($n = 4$ for Br). Its value has been determined for both Br isotopes by King and Jaccarino [21] from an atomic beam magnetic resonance experiment. Their values are − 769.756 MHz for ^{79}Br and − 643.033 MHz for ^{81}Br.

Within a simple valence shell LCAO molecular orbital model [22] in which all nuclear contributions to the electric field gradient are neglected and in which only the one center integrals located at the Br nucleus are retained for the calculation of the quadrupole coupling tensor elements, δ as defined by (5) would be equal to the population difference in the bromine $4\,p_x$ and $4\,p_y$ orbitals i.e.

$$\delta = P_{p_z p_z} - P_{p_y p_y} = 2 \sum_{m}^{\text{occ. orb.}} (c^2_{m p_x} - c^2_{m p_y}). \tag{6}$$

Table 6. Double bond character in the carbon halogen bond of several unsaturated hydrocarbons as derived from the halogen nuclear quadrupole coupling constants according to Eq. (6) of the text. The value of 0.009 (or 0.9% double bond character) for 2 chlorothiopene is recalculated. It follows from the quadrupole coupling constants listed in Table 5 of [22] which have been checked by us to reproduce the list of experimental splittings. The value of 0.006 given by the authors appears to be a printing error.

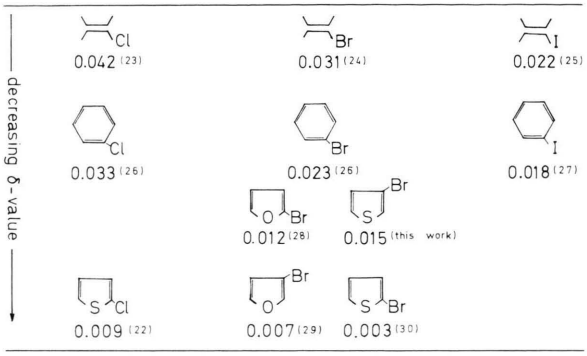

In (6) c_{mp_x} is the coefficient of the bromine valence shell p_x orbital in the m-th molecular orbital. The sum runs over all occupied space orbitals and the factor of 2 accounts for occupation of each orbital with two electrons with antiparallel spins.

In Table 6 we list the δ-values calculated from (5) together with the corresponding values for several other aromatic systems. Also listed for comparison are the δ-values for the corresponding vinylhalides. First we note that there is a trend to increasing double bond character in the carbon-halogen bond when proceeding from I- to Cl-substitution. This trend parallels the improving overlap properties of the out of plane halogen p_y-orbitals with the out of plane p_y-orbital of the adjacent carbon atom.

However, we must also note two facts which still call for an explanation. First, the double bond character in the CBr bond of vinylbromide is larger than in bromobenzene while it is smaller in the substituted furanes and thiophenes. At first sight one would expect a trend in the same direction when changing from a delocalized system (benzene) to a system with a more localized double bond adjacent to the CBr bond i.e. one would expect the furanes and thiophenes to hold an intermediate position.

Second there is a marked difference in the double bond character of the α-substituted and of the β-substituted heteroaromates, but with opposite trends for the furanes and for the thiophenes. While α-bromofurane shows twice the double bond character of β-bromofurane, β-bromothiophene shows about three times the double bond character of α-bromothiophene. This effect is well above the experimental uncertainties in the δ-values which are on the order of ± 0.001 as is also seen in the consistency of the results for the two bromine isotopes. Our problems in understanding the data may of cause merely indicate that the simple LCAO-model upon which our interpretation of the quadrupole coupling constants is based, has been pushed beyond its limits of approximation if double bond characteres of the order of only one to four percent are discussed.

Acknowledgements

We thank V. Typke who provided his program ZFAP4 for the centrifugal distortion analysis. We further thank professors H. Dreizler and A. Guarnieri for reading the manuscript. The financial support from Deutsche Forschungsgemeinschaft and Fonds der Deutschen Chemischen Industrie is gratefully acknowledged. All numerical calculations were carried out at the Computer Center of the University of Kiel.

[1] D. Hübner, M. Stolze, and D. H. Sutter, Z. Naturforsch. **36 a,** 332 (1981).
[2] D. Hübner, M. Stolze, and D. H. Sutter, Z. Naturforsch. **37 a,** 95 (1982).
[3] W. H. Stolze, M. Stolze, D. Hübner, and D. H. Sutter, Z. Naturforsch. **37 a,** 1165 (1982).
[4] Yoshiaki Sasada, Nasazi Saitoh, and Shinich Tobita, J. Mol. Spectr. **92,** 363 (1982).
[5] G. Bestmann and H. Dreizler, Z. Naturforsch. **37 a,** 58 (1982).
[6] G. Bestmann, H. Dreizler, H. Mäder, and U. Andresen, Z. Naturforsch. **35 a,** 392 (1980).
[7] Dieter Ziessow, One-Line Rechner in der Chemie, Abschnitt 2.2.2., Walter de Gruyter, Berlin 1973.
[8] B. Bak, D. Christensen, L. Hansen-Nygaard, and S. Rastrup-Andersen, J. Mol. Spectry. **7,** 58 (1961).
[9] E. Rosenthal and B. P. Daily, J. Chem. Phys. **43,** 2093 (1965).
[10] T. Ogate and U. Kozima, J. Mol. Spectry. **42,** 38 (1972).
[11] Handbook of Chemistry and Physics, 62nd. edition, CRC-Press (1981).
[12] M. Stolze, D. Hübner, and D. H. Sutter, Z. Naturforsch. **36 a,** 886 (1981).

[13] For the principle of this perturbation treatment see for instance Chapt. 3 in H. C. Allen jr. and P. C. Cross, Molecular VIB-Rotors, John Wiley and Sons, Inc., New York 1963.
[14] B. P. van Eijck, J. Mol. Spectry. **53,** 246 (1974).
[15] Volker Heine, Group Theory in Quantum Mechanics, p. 199, Pergamon Press; London 1960.
[16] H. P. Benz, A. Bauder, and Hs. H. Günthard, J. Mol. Spectry. **21,** 156 (1966).
[17] H. D. Rudolph, Z. Naturforsch. **23 a,** 540 (1968).
[18] Diplomtheses of M. Stolze and D. Hübner, Kiel 1980.
[19] W. Gordy and R. L. Cook, Microwave Molecular Spectra, Chapt. 14.11.c. Interscience Publishers, New York 1970.
[20] J. H. Goldstein, Chem. Phys. **22,** 2078 (1954).
[21] J. G. King and V. Jaccarino, Phys. Rev. **94,** 1610 (1954).
[22] J. Mjöberg and S. Ljunggren, Z. Naturforsch. **28 a,** 729 (1973).
[23] M. C. L. Gerry, Can. J. Chem. **49,** 255 (1971).
[24] D. de Kerckhove Varent, Ann. Soc. Sci. Bruxelles **84,** 227 (1970).
[25] M. J. Moloney, J. Chem. Phys. **50,** 1981 (1969).
[26] W. Caminati and A. M. Mirri, Chem. Phys. Lett. **12,** 127 (1971).
[27] W. Caminati and A. M. Mirri, Chem. Phys. Lett. **8,** 409 (1971).
[28] M. Stolze, Diplom-Thesis, University of Kiel 1980.
[29] D. Hübner, Diplom-Thesis, University of Kiel 1980.
[30] P. J. Mjöberg, W. M. Ralowski, and S. O. Ljunggren, Z. Naturforsch. **30 a,** 541 (1975).
[31] J. K. G. Watson, Aspects of Quartic and Sextic Centrifugal Effects on Rotational Energy Levels, in Vibrational Spectra and Structure, (J. R. Durig, ed.), Vol. 6, Elsevier Amsterdam 1977, (see page 73, S-reduction, representation I^r. Van Eijck's and Watson's parameters correlate as follows:
$D'_J = D_J$, $D'_{JK} = D_{JK}$, $D'_K = D_K$, $\delta'_J = -d_1$, $R'_6 = d_2$).
[32] H. Jones and V. Typke, Z. Naturforsch. **36 a,** 1057 (1981).